DOI: 10.13009/EUCASS2023-677
Aerospace Europe Conference 2023 – 10TH EUCASS – 9TH CEAS

GNSS relative navigation for operations in cislunar space

Marco SABATINI†, Paolo GASBARRI*, Giovanni B. PALMERINI**

** Scuola di Ingegneria Aerospaziale, Sapienza Università di Roma*
Via Salaria 851 – 00138 Roma, Italy
marco.sabatini@uniroma1.it, paolo.gasbarri@uniroma1.it, giovanni.palmerini@uniroma1.it
† Corresponding Author

Abstract

This paper investigates the performance of the forthcoming lunar navigation satellite systems for estimating not only the position of an onboard receiver in a lunar inertial reference frame, but also, and with a consistent accuracy, the relative position between two or more spacecraft in proximity. This could be the case of two spacecraft performing a rendezvous, of a lander released by an orbiter or the case of the permanent relative navigation service for a formation of satellites around the Moon. A cascade Kalman filter is implemented and the performance in terms of error statistics are shown for different mission profiles.

1. Introduction

Satellite formations have proven to be instrumental in various space missions, enabling collaborative data acquisition, improved mission robustness, and enhanced scientific investigations. With the renewed interest in the exploration of the Moon [1] the deployment of satellite formations in lunar orbits [2] can be of great interest for comprehensive studies. However, precise navigation and coordination of satellites within these formations poses unique challenges due to the absence of lunar GNSS systems, the expected limited capabilities of these spacecraft, the insufficient possibilities of Earth-based tracking.
The possibility to offer a navigation service similar to GPS or GALILEO navigation systems, even in a reduced scale and limited performance, has been recently carried on by many studies [3]. Both NASA and ESA, with the Lunanet [4] and Moonlight [5] mission concepts are making rapid progress in the development of dedicated GNSS systems for the navigation of both lunar rovers and orbiters. The constellation dedicated to navigation could be selected among well-known orbital design families, such as Walker orbits, Elliptical Lunar Frozen orbits (ELFO), Earth-Moon Libration Points orbits [6]. The ELFO constellation offers high stability of the orbital parameters, suitable to cover poles area and low station keeping budgets, and is therefore the baseline solution in the current studies [7].
Because of the reduced number of satellites of the constellation, the design of the formation is optimized for specific mission and specific areas of interest, which usually are related to rovers and landers in the Moon South Pole region. This paper investigates the possibility to extend the use of these navigation signals to the estimate of relative state of a formation of two or more satellites in Moon orbit.
A “cascade of filters” approach is employed: the first filter stage focuses on estimating the position of each satellite of the formation in the Moon inertial frame, leveraging pseudorange and pseudorange rates measurements and accounting for the complex gravitational influences and perturbations encountered in the lunar environment. This first extended Kalman filter can provide estimates that can be considered satisfactory for the individual satellite orbit determination but could prove insufficient when directly used to compute the relative state, with large percentage errors with respect to the formation baseline. A second filtering stage is therefore implemented, designed to estimate the relative position between satellites within the formation. By incorporating inter-satellite dynamics, this filter leverages the inertial position estimates of the first filtering stage to achieve a final relative state estimation which is less affected by the lack of a sufficient number of navigation signals, which periodically happens (because of the reduced number of navigation satellites).
To validate the performance of our proposed navigation system, extensive simulations and analysis are conducted. The accuracy, convergence, and robustness of the cascade of filters approach is evaluated, considering different scenarios and mission profiles. Even though the performance is deeply affected by the initial configuration of the navigation constellation, by the formation baseline dimension, and by random errors affecting the original measurements (i.e. the

DOI: 10.13009/EUCASS2023-677

pseudoranges), this paper contributes to offer a first qualitative evaluation of the possible additional use of a lunar GNSS system.
The paper is organized as follows: Section 2 introduces the constellation devoted to navigation services; Section 3 describes the performance of an Extended Kalman filter leveraging the available pseudoranges. Section 4 deals with the original contribution of the paper, i.e. the relative navigation filter, whose results are reported in Section 5. Final remarks can be found in Section 6.

2. Elliptical Lunar Frozen Orbit (ELFO) constellation

The orbital parameters of the satellites of the ELFO constellation for satellite navigation [8] are selected to provide high stability, significant coverage of poles areas (in particular the South pole) while requiring low station keeping budgets and minimizing orbit maintenance costs.
Opposite to ref. [9] where a constellation of 5 satellites was considered, four ELFO satellites in three different orbital planes are considered (as in [6] and [7]) in this work. This is a minimum for satellite navigation, thus the performance obtained with this minimum configuration could only improve if larger constellations should be considered. The selected parameters are described in Table 1, the resulting orbits (propagated in a Moon Inertial frame[1]) are reported in Figure *1*.

Table 1 Initial ELFO constellation parameters.

	SAT 1	**SAT 2**	**SAT 3**	**SAT 4**
a (km)	9750.7	9750.7	9750.7	9750.7
ecc	0.69	0.69	0.69	0.69
Incl (deg)	55.7	55.7	55.7	55.7
Arg.Perilune (deg)	90	90	90	90
RAAN (deg)	0	-120	120	120
f_0 (deg)	0	61.7	45.5	180

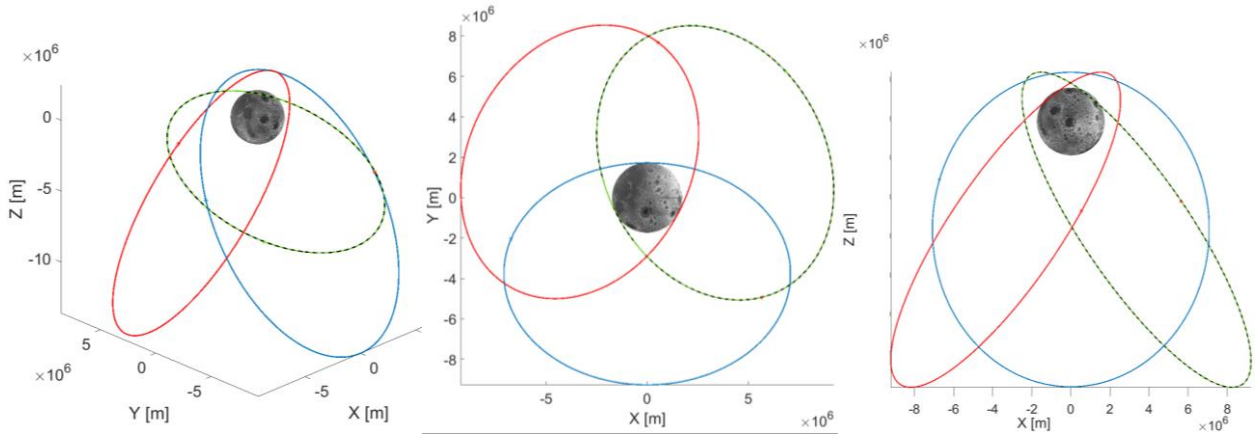

Figure 1: 3D (left figure), equatorial projection (XY, middle figure) and XZ projection (right figure) of the ELFO constellation in the Moon Inertial reference frame.

A simplified model is adopted for assessing the visibility of an ELFO satellite from a receiver, only relying on geometrical considerations. A navigation signal is considered received if:

i. the vector from the ELFO satellite to the receiver is not blocked by the Moon (plus a 50km mask altitude);
ii. the vector from the ELFO satellite to the receiver is inside a 15-degrees semi-aperture cone representing the transmitting antenna pattern.

[1] The Moon Inertial frame, centered in the Moon, is defined as an inertial system referenced to the Moon equator (at the J2000 epoch) with x-axis pointing along the line formed by the intersection of the Moon equator and Earth's mean equator at J2000. The z-axis points along the Moon's spin axis direction at the J2000epoch. The y-axis completes the right-handed set.

DOI: 10.13009/EUCASS2023-677

As an example, referring to Figure 2, the orbiter has visibility of ELFO satellites C and D (the unit vectors from ELFO satellites to the orbiter fall inside the antenna main lobe), while it does not have visibility of satellites A (relative position vector outside the main lobe) and B (relative vector would be inside the lobe, but the Moon body is between the orbiter and the satellite).

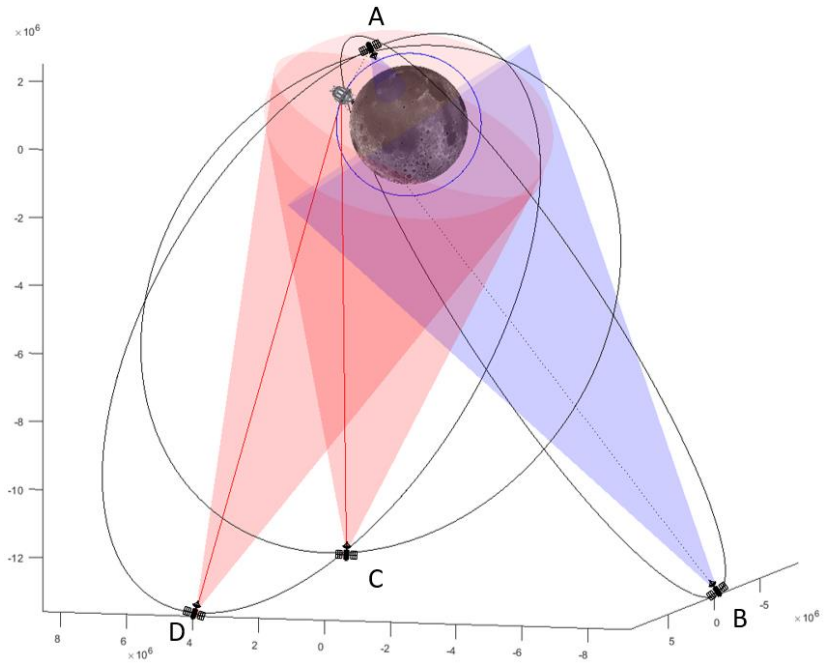

Figure 2: Geometric visibility conditions

3. Moon inertial state estimation

As explained in [8], ranging code and navigation messages should be broadcasted by the satellites and then exploited by the user to compute its own position, inverting the navigation equations. In this way, the user receiver could exploit all the already tested and robust GNSS receiver approaches to compute its own position.
As well-known, at least four satellites would be necessary to algebraically compute the receiver position (and associated clock delay). In a lunar system made of just four satellites, the time availability of all satellites is quite limited and calls for an estimation of the state to extend the navigation also when availability is much lower. At the scope, a filter can be developed, which is however not the main interest of the study; it will be briefly explained, while its performance and limitations, together with its possible improvements are left to parallel publications [10][10].
As explained shortly after, the measurement equations are nonlinear, and therefore an Extended Kalman Filter (EKF) will be implemented. For each tracked satellite, the usual steps of EKF are performed [11], i.e.:

1) Initialization
2) Propagation
3) Kalman gain computation
4) Update

The state to be estimated includes the receiver kinematic state (position and velocity in the Moon inertial frame) and the receiver clock error, defined as a clock bias, c_0 and a clock drift c_1.

$$X = [X_r \quad Y_r \quad Z_r \quad \dot{X}_r \quad \dot{Y}_r \quad \dot{Z}_r \quad c_0 \quad c_1] \tag{1}$$

Here and in the following *hat* symbol stands for estimated quantities, while *tilde* symbol stands for predicted quantities. In the propagation phase both the state and the associated error covariance matrix P are propagated over a time step $\Delta T=t_k-t_{k-1}$, starting from a previous estimate, $\hat{X}_{k-1}$ and $\hat{P}_{k-1}$ respectively.

$$\begin{aligned} \tilde{X}_k &= \hat{X}_{k-1} + \int_{t_{k-1}}^{t_k} f(X,t)dt \\ \tilde{P}_k &= \Phi_k \hat{P}_{k-1} \Phi_k + Q_k \end{aligned} \tag{2}$$

DOI: 10.13009/EUCASS2023-677

The equations used for the propagation of the satellite state are provided by the orbital dynamics of a body around the Moon:

$$\dot{X} = f(X,t) \tag{3}$$

where $f(X,t)$ includes the first 20 harmonics of the Moon gravitational potential, the gravitational attraction of the Earth and the solar radiation pressure [11]. The more accurate is the dynamics, the lower is the so-called process error, or Q_k ; at the same time, the larger is the computation time. In fact, together with the state, also the associated covariance matrix P must be propagated; a transition matrix $\Phi_k = e^{F_k \cdot \Delta t}$ is required, where the linearized state matrix $F_k = \frac{\partial f(X_k, t_k)}{\partial X_k}$ must be numerically computed at each time step, further increasing the computation cost.

The measurements are the usual quantities of GNSS: pseudorange p_r^s and pseudorange rates $\dot{p}_r^s$, which are a nonlinear function of the state $[\, p_r^s \quad \dot{p}_r^s \,] = h(X)$:

$$\begin{aligned} p_r^s &= \left\| r_r^s \right\| + \delta t + \varepsilon_r^s \\ \dot{p}_r^s &= \| \dot{r}_r^s \| + c_1 + \dot{\varepsilon}_r^s \end{aligned} \tag{4}$$

where r_r^s is the difference between the satellite r_s and the receiver r_r position vectors; $\dot{r}_r^s$ is the difference between the satellite $\dot{r}_s$ and the receiver $\dot{r}_r$ velocity vectors; δt is the clock error modelled with a linear model: $\delta t = c_0 + c_1 t$, where c_0 is the clock bias and c_1 is the clock error drift. Finally, ε_r^s and $\dot{\varepsilon}_r^s$ are the pseudorange and pseudorange rate noises, modelled as random gaussian noise with standard deviation equal to 15m and 0.15m/s, respectively.

The measurement equation (4) can be used to compute the predicted measurements $h(\tilde{X}) = [\tilde{p}_r^s \quad \dot{\tilde{p}}_r^s]$. A linearization of the measurement equation is needed for the computation of the Kalman gain. The dimensions of the measurement matrix H_k is $2N_{sat}$ x 8, where N_{sat} is the number of ELFO satellites visible at time t_k (ranging from 1 to a maximum of 4). If no navigation satellite is in visibility, it means that no measurement is available, so the update phase is not run and the estimate coincides with the propagated state. In all other cases, each $2x8$ block of H_k reads as:

$$H_k^i = \begin{bmatrix} a_x^s & a_y^s & a_z^s & 0 & 0 & 0 & 1 & 0 \\ \dot{a}_x^s & \dot{a}_y^s & \dot{a}_z^s & a_x^s & a_y^s & a_z^s & 0 & 1 \end{bmatrix} \tag{5}$$

where $a_{x,y,z}^s$ are the direction cosines of the vector from the satellite s to the receiver, and $\dot{a}_x^s = -\frac{\dot{X}_S - \dot{X}}{\|r_r^s\|} + \frac{X_S - X}{\|r_r^s\|^2} \dot{r}_r^s$ (and similarly for components along Y and Z). This matrix H_k is used to compute the Kalman gain:

$$K_k = \tilde{P}_k H_k^T \left(H_k \tilde{P}_k H_k^T + R_K \right) \tag{6}$$

which is then introduced in the update equations, for computing the estimate:

$$\begin{aligned} \hat{X}_k &= \tilde{X}_k + K_k \left(z - h(\tilde{X}) \right) \\ \hat{P}_k &= (I - K_k H_k) \tilde{P}_k \end{aligned} \tag{7}$$

The performance of the navigation system of the single satellite deeply affects the relative navigation system that is the main focus of this research. Therefore, two scenarios are analyzed in the following: the first case when a quite rough initialization is provided, and a second one when stationary estimate behavior is reached. In both cases the reference orbit of the receiver is a circular orbit, with semimajor axis a = 2125 km, i.e. almost 400 km altitude above the lunar surface (mean radius of the Moon 1737.4 km), and inclination i = 85 deg.

3.1 Case 1: Cold start

In this first simulation, the performance in terms of positioning error of the estimate is analyzed starting from the following initial condition, including a relevant error:

$$\hat{X}_0 = X + randn \cdot E_0 \tag{8}$$

DOI: 10.13009/EUCASS2023-677

where *randn* indicates a gaussian random distribution of variance equal to one, while E_0 is the initial error in the state (assumed equal to 10 km on each axis for position, 10 m/s on each axis for velocity, 1km for clock bias and 0.1 m/s for clock error drift).
The time needed for achieving convergence mainly depends on the initial true anomaly of the ELFO satellites, allowing (or not) a full availability of the constellation in a short time. The first simulation is purposely run with a particularly unlucky initial configuration of the ELFO, which allows full visibility of the constellation only for a short period at the end of the simulation (see Figure 3). Therefore, the position error is of the order of tens of kilometers for long time, showing, as expected, that the implemented EKF cannot converge if no satellites or only one satellite are in visibility. The estimate error quickly improves when more satellites are in visibility, ending with a very good accuracy after initialization is over (see the paragraph 3.2 for the performance at stationary). As reported in Figure 4, the convergence would have been much quicker if the initial ELFO had been soon allowed for a full visibility.

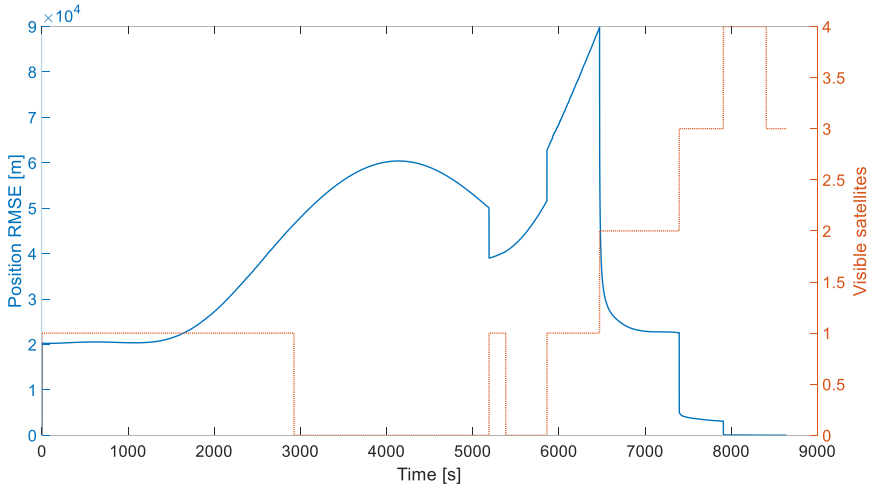

Figure 3: Norm of the error following a cold start of the inertial navigation filter in the *unlucky case* (see the low initial number of visible satellites).

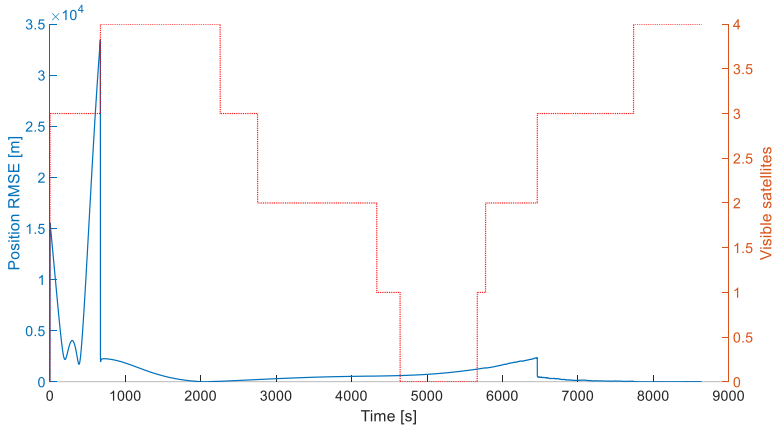

Figure 4: Norm of the error following a cold start of the inertial navigation filter in a *lucky case* (see the large initial number of visible satellites).

3.2 Case 2: Performance at stationary

Let us now suppose that the initialization has been already performed, so the simulation has a very low initial error (actually equal to zero, for simplicity), and runs for 12 hours, so that it is possible to analyze the performance over a longer time. It is possible to see from Figure 5 that the periodic (in particular in the passages over the South Pole) full visibility of the ELFO satellites allows for a very low position error (order of few meters). On the other side, during the time intervals when only one or even zero satellites are in visibility - in the latter case only the Kalman filter is limited to the propagation, as no measurements are available for the update phase - there is an increase in the error, attaining a peak value of 300 m. The mean value of the error (computed in terms of position error norm) is 19 m.

DOI: 10.13009/EUCASS2023-677

The periodic increase and decrease in the estimate error can be also evaluated from the value of the associated covariance matrix. In Figure 6 the error of one of the components of the estimated position vector is plotted together with the corresponding element of the covariance matrix: it is possible to see that periodically the covariance matrix converges and then increases again because of the reduced number of measurements.

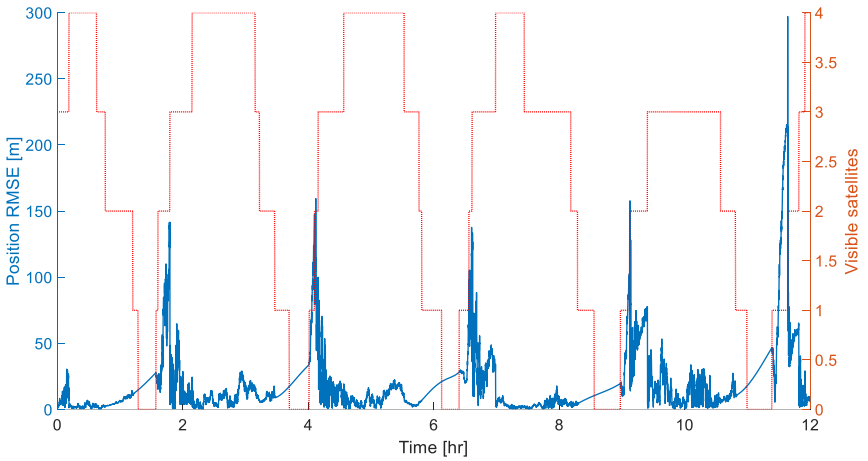

Figure 5 : Norm of the error of the inertial navigation filter at stationary.

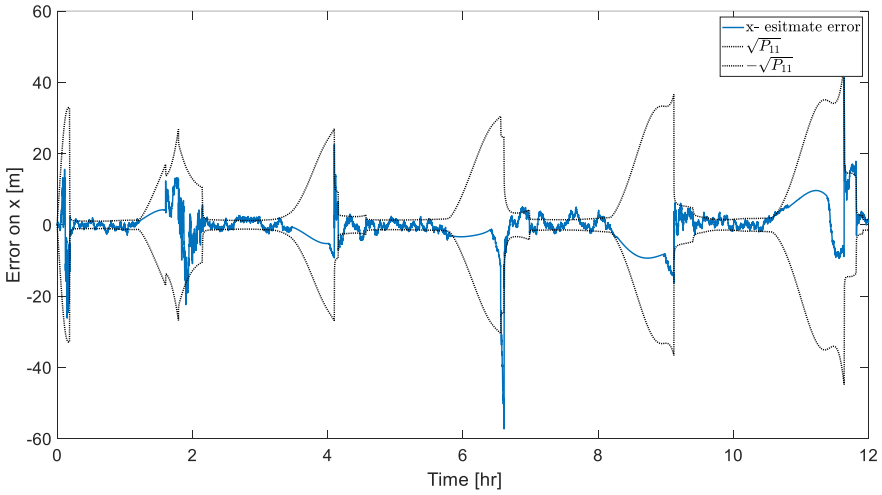

Figure 6 : Error of one estimate component in the inertial frame,
together with the associated covariance matrix element.

4. Relative motion

4.1 Relative motion scenarios

The case of relative state estimation is now analyzed more in detail. The problem can be of interest in the case of missions including a rendezvous in the cislunar space, in the case of separation of a lander from an orbiter, or in the case of a continuous operation of a fleet of two or more spacecraft, for example devoted to remote sensing. Three relative orbital configurations are considered as representative of the different possible missions:

- Scenario A: the orbits of the two satellites of the formation have the same semiaxis and a different eccentricity, (the so-called cartwheel configuration). This results in an elliptical relative motion (plotted in a Local Vertical Local Horizontal (LVLH) frame, with x-axis aligned with orbital radius, z aligned with angular velocity, and y completing the right-handed reference frame), as in
- Figure *7*a;

DOI: 10.13009/EUCASS2023-677

- Scenario B: the two satellites (e.g., a lander and an orbiter) are initially on the same circular orbit, but at *t=0s* an impulsive tangential ΔV is applied for the separation of the lander, which is from now on an orbit with different semiaxis. As a result, a drift in the along-track direction is the main component of the relative motion (see
- Figure *7*b);

- Scenario C: the two satellites are in the same circular lunar orbit, with a large phase angle difference. The resulting relative trajectory is a limited motion (ideally constant if no perturbations were included, see
- Figure *7*c)

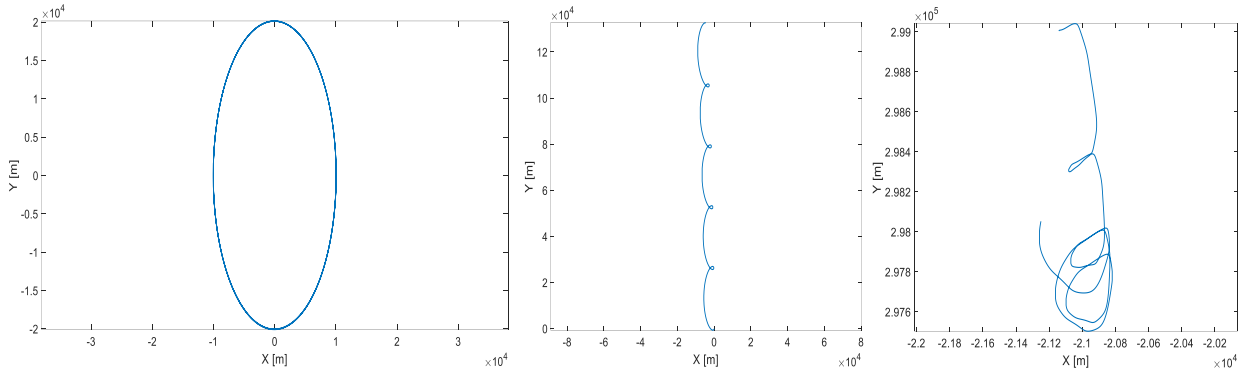

Figure 7: Cartwheel formation (subplot *a*), drifting formation at separation (subplot *b*) and train formation (subplot *c*) trajectories projected in the local vertical plane of the frame centered at the chaser.

4.2 Relative state from inertial state estimate

It is supposed that a communication link is available between the spacecraft of the formation, so that the information of the estimated position in the moon inertial frame, as computed in Section 3, can be shared.
Therefore, as soon as the inertial position of the two satellites is available, the relative state (in the LVLH frame) can be algebraically computed as follows.
Given the position X_1, X_2 of the two satellites of the formation, and the orbital parameters oe_1 of the satellite identified with number 1, the relative position can be computed as:

$$\overset{\mathrm{r}}{\rho} = T\left(oe_1\right)\left(X_2 - X_1\right) \tag{9}$$

Let us consider the case of Scenario A. The estimation procedure in Section 3 is run at each time step for the two satellites independently. The resulting estimates, $\hat{X}_1, \hat{X}_2$, are computed, together with the (estimated) orbital parameters $\hat{o}e_1$. In the frame of a numerical simulation, it is possible to directly compute the (estimated) relative distance, and compare the results with the true relative distance.
Following Figure 8 shows the norm of the error on the relative position obtained in this direct algebraic way. It is possible to see that, as for the single satellite case, also the relative state suffers from large periodical peaks of errors.
The mean error resulting from the simulation reported as an example is 24 m, while the maximum error is as large as 200 m. Such an order of magnitude of the errors can be considered acceptable for the estimate of the orbital parameters while independently tracking each satellite, but is likely to be inadequate for performing formation flying navigation and control operations. In fact, these values corresponds to errors up to 1% of the formation baseline in the present case. With the aim of limiting this problem, a second filter, purposely developed for estimating the relative state can be developed and applied considering the so called cascading approach.

DOI: 10.13009/EUCASS2023-677

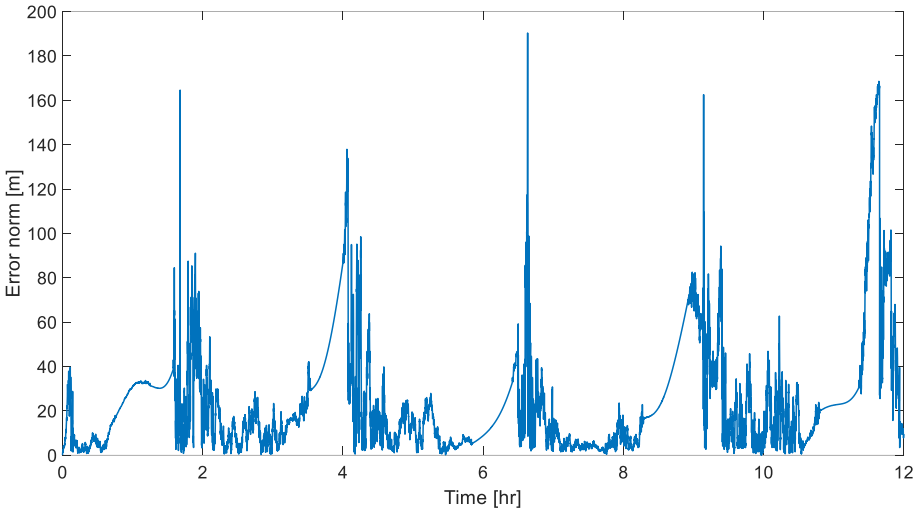

Figure 8 Relative distance error norm as computed using the two inertial navigation filters

4.3 Relative Navigation architecture

A Kalman filter is implemented also for the relative dynamics estimation. The fundamental steps are formally the same as in the previous paragraph, but of course with different dynamics model and measurement equations.
There are several ways to model the relative motions of two spacecraft; relative coordinates in the LVLH frame are certainly one of the most intuitive and they allow for an immediate comprehension of the motion. However, dynamics models based on cartesian coordinates suffer from linearization ([12],[13]) or they become hard to model when perturbations are included; additionally, the coordinates are by nature varying with orbital period. When relative orbital parameters are used, instead, their behavior is nearly constant and perturbations are much easier to be included [14]; they do not suffer from linearization, but they provide information that do not immediately allow for the interpretation of the motion.
Therefore, the set of differential orbital parameters described in [15] is used as relative state to be estimated, defined as:

$$\delta\alpha = f\left(\alpha_d, a_c, i_c\right) - f\left(\alpha_c, a_c, i_c\right) = \left(\delta a, \delta\lambda, \delta e_x, \delta e_y, \delta i_x, \delta i_y\right) \tag{10}$$

with

$$f\left(\alpha\ , a_c, i_c\right) = \begin{pmatrix} a/a_c \\ u + \Omega\cos i_c \\ e\cos\omega \\ e\sin\omega \\ i \\ \Omega\sin i_c \end{pmatrix}$$

while for visualization purposes they are transformed in relative coordinates. For simplicity, all the *differential* perturbations (third body attraction, higher harmonics of the moon gravitational potential, solar radiation pressure) are for the moment neglected, therefore the resulting dynamics simply reads as:

$$\dot{\delta}\alpha = \begin{bmatrix} 0 & \sqrt{\frac{\mu}{a_2^3}} - \sqrt{\frac{\mu}{a_1^3}} & 0 & 0 & 0 & 0 \end{bmatrix} \tag{11}$$

Being μ the Moon gravitational parameter. The dynamics model is only slightly nonlinear, and for short distances (qualitatively below 100km), also the linearized version can be used:

DOI: 10.13009/EUCASS2023-677

$$\dot{\delta\alpha} = \begin{bmatrix} 0 & -\frac{3}{2}\sqrt{\frac{\mu}{a_1^3}}\delta\alpha & 0 & 0 & 0 & 0 \end{bmatrix} \tag{12}$$

The input of the filter cannot be properly defined as measurements' set, since it is actaully a mathematical manipulation of the estimates of the navigation system of the two satellites:

$$z_{rel} = \delta\alpha_{input} = g\left(\hat{o}e_1, \hat{o}e_2\right) = k\left(\hat{X}_1, \hat{X}_2\right) \tag{13}$$

In other words, a cascade filter architecture is realized, as shown in Figure 9.

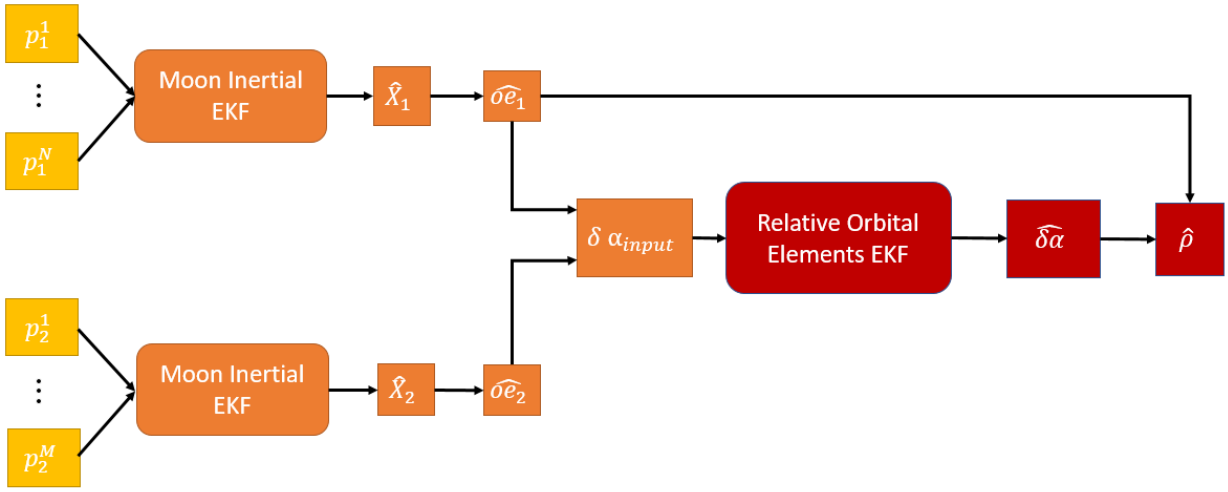

Figure 9 : Cascade filter architecture implemented for relative state estimation

While the covariance matrix associated to the noise on the original measurements is clearly related to the noise of the pseudoranges and pseudorange rates, the covariance matrix of the input of the relative dynamics filter, z_{rel}, is not straightforward to define. In fact, it depends on the error on the estimates of the first two filters in a highly nonlinear way. In order to compute at each timestep the value of the covariance matrix associated to the error of $\delta\alpha_{input}$, indicated as R_{rel}, an unscented transformation is applied ([16], [176]). Let us define:

$$\hat{X}_{inertial} = \begin{bmatrix} \hat{X}_1 & \hat{X}_2 \end{bmatrix} \tag{14}$$

the estimate of the inertial positions of the two satellites belonging to the formation, and

$$P_{inertial} = \begin{bmatrix} P_1 & 0 \\ 0 & P_2 \end{bmatrix} \tag{15}$$

the associated error covariance matrix. The first step consists in computing $2n$ sigma points (with $n = 12$)

$$\begin{aligned} \hat{X}^{(i)}_{inertial} &= \hat{X}_{inertial} + \left(\sqrt{nP_{inertial}}\right)^T_i, \quad \text{with } i = 1,\ldots,n \\ \hat{X}^{(n+i)}_{inertial} &= \hat{X}_{inertial} - \left(\sqrt{nP_{inertial}}\right)^T_i, \quad \text{with } i = 1,\ldots,n \end{aligned} \tag{16}$$

DOI: 10.13009/EUCASS2023-677

where $\sqrt{nP_{inertial}}$ is the matrix square root of $nP_{inertial}$ (computed with a Cholesky decomposition) and $\left(\sqrt{nP_{inertial}}\right)_i$ is the *i-th* row of $\sqrt{nP_{inertial}}$. The nonlinear transformation of the *2n* sigma points is defined as:

$$\delta\alpha_{input}^{(i)} = k\left(\hat{X}_{inertial}^{(i)}\right) \tag{17}$$

The mean $\bar{\delta\alpha}_{input}$ of the transformed sigma points can be evaluated and the associated error covariance matrix of the input to the relative orbital elements filter finally computed as:

$$R_{rel} = \frac{1}{2n}\sum_{i=1}^{2n}\left(\delta\alpha_{input}^{(i)} - \bar{\delta\alpha}_{input}\right)\left(\delta\alpha_{input}^{(i)} - \bar{\delta\alpha}_{input}\right)^T \tag{18}$$

Figure *10* reports as an example the error of the first component of the input vector $\delta\alpha_{input,1}$, together with the first component of the associated error covariance matrix.

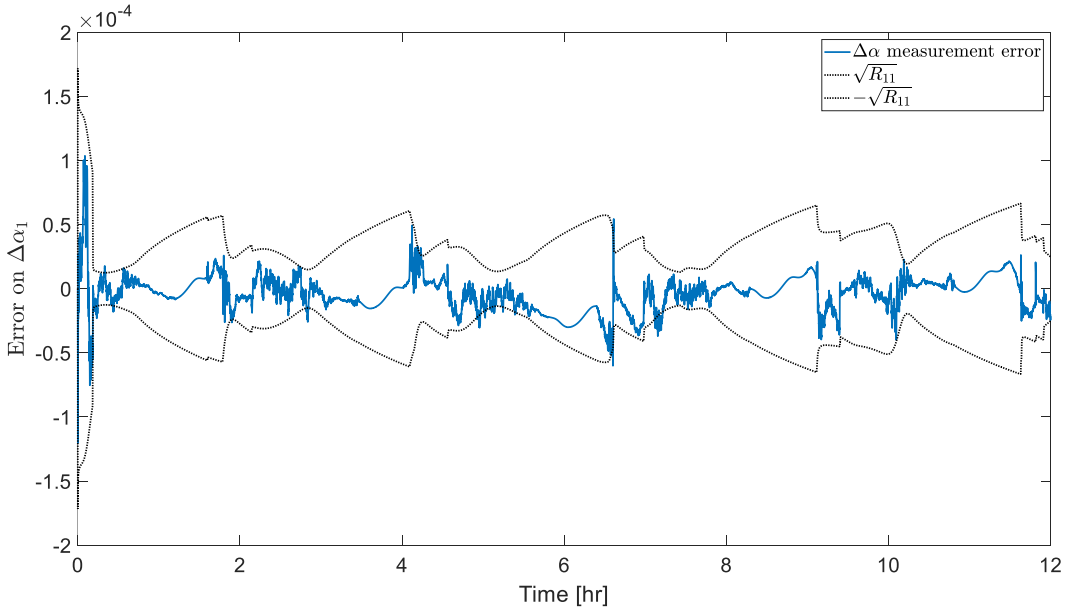

Figure 10 : Error on the first element of the state vector (differential normalized semimajor axis), together with the associated covariance matrix element, computed as unscented transform of the covariance matrices of the inertial state estimates.

5. Results

The three scenarios of Section 4.1 are considered for analyzing the performance of the navigation cascade filter.
Figure *11* reports the error in the state components of the estimate (red) and of the input (blue). As already stated, while it could seem clear at a glance that the final estimate vector is much smoother and with less pronounced peaks, a clear assessment in terms of relative position error is missing. For that, the input and the estimated relative orbital elements can be transformed in relative cartesian coordinates in the LVLH frame.
Figure *12* shows the position error norm of the input and of the estimate. The mean value of the estimate error is 17 m (with respect to 24 m of the input) and a maximum value of 84m (with respect to 190 m of the input). Therefore, it is possible to affirm that in the analyzed case the improvement is remarkably evident in the reduction of the maximum errors, which are reduced by approximately 55%, while a reduction of 30% is achieved on the mean value.

DOI: 10.13009/EUCASS2023-677

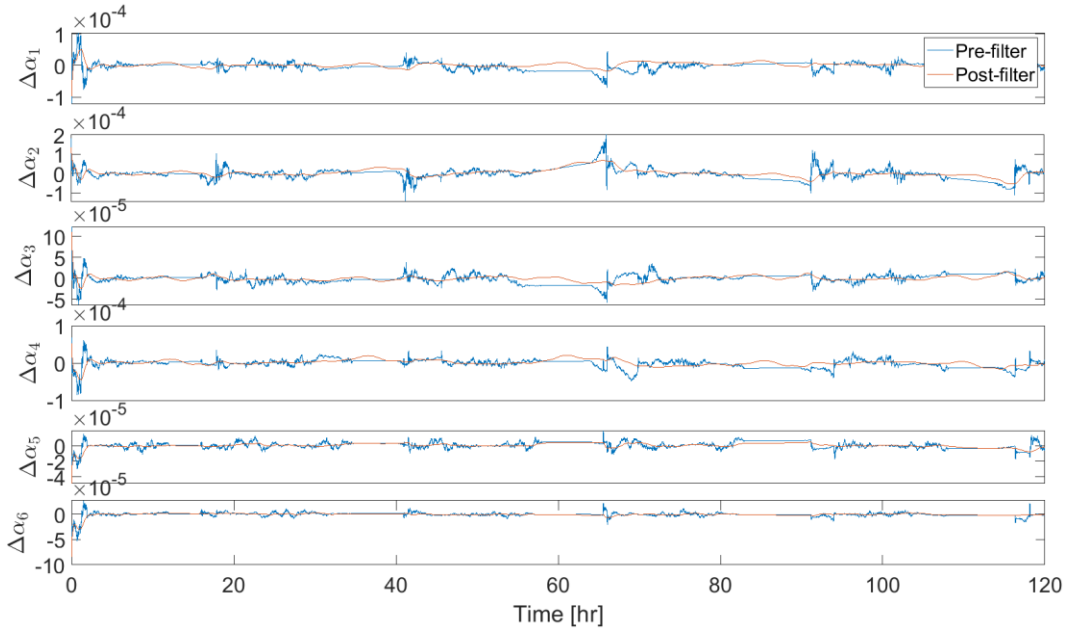

Figure 11: Error of the input and estimated elements of the relative state.

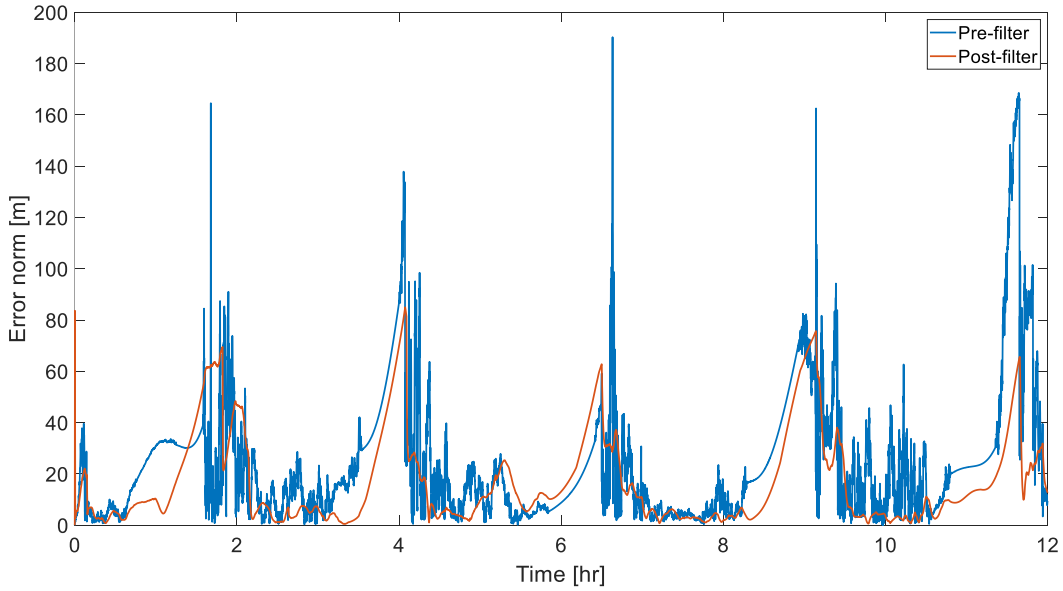

Figure 12 : Norm of the error of the input and estimated relative position

As already stated in Section 3, these results also depend on the specific initial configuration of the ELFO satellites, but the long duration of the simulation (12 hours) should reduce such a significant effect. The relative navigation performance is however affected also by the random noise of the pseudoranges, and thus it suffers from a large variation from simulation to simulation, in particular on the maximum values, as it is possible to see from
Figure *13*, which is relevant to a 50 runs Monte Carlo simulation. The mean value for all these simulations is plotted in
Figure *14*, with a median value of 17m and a maximum value of 42m.

DOI: 10.13009/EUCASS2023-677

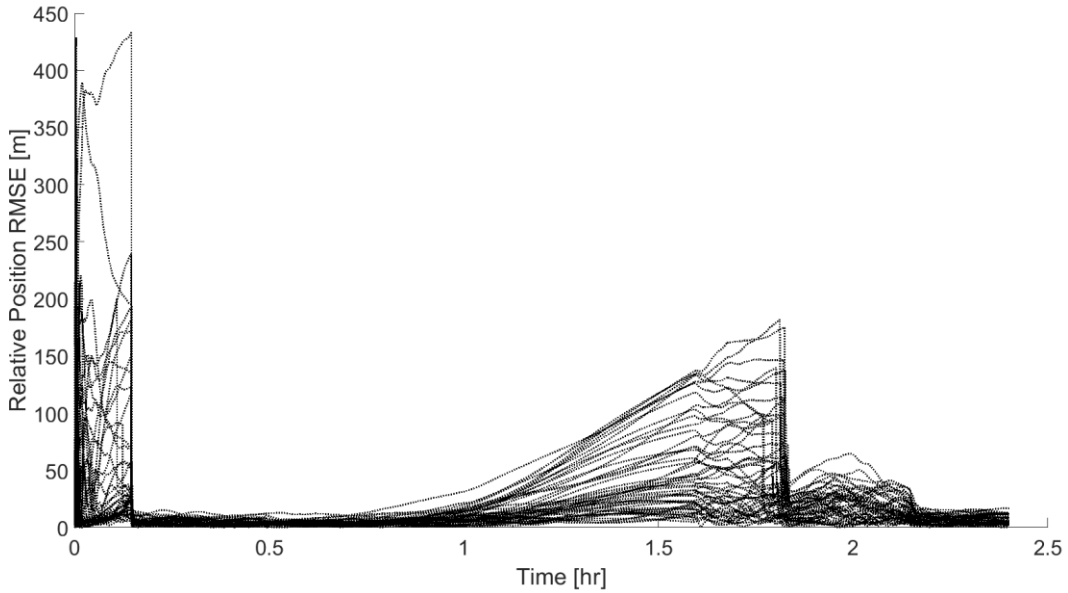

Figure 13 : Norm of the error of the estimated relative position in 50 simulations run with different random errors affecting the pseudoranges.

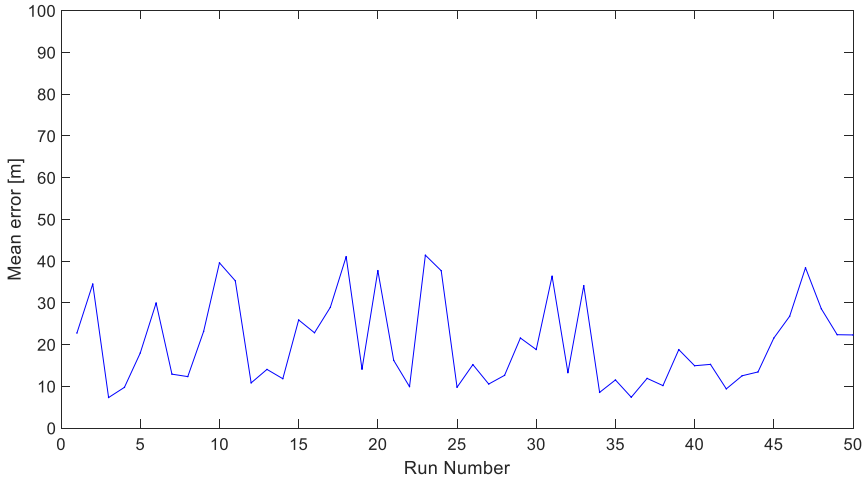

Figure 14 Mean error recorded during a 50 runs Monte Carlo simulation

Also, the specific orbit of the receivers affects the visibility of the ELFO satellites and thus the performance of the relative navigation consequently depends on the orbital configuration. An extensive study of a vast number of orbital sets is outside the scope of the present paper. The attention is focused on the parameter that is more likely to affect the performance, i.e., the inclination of the orbit. In fact, the ELFO constellation is designed to maximize the coverage of the South Pole region; polar orbits periodically benefit from the maximum visibility, but at the same time the suffer from maximum outage. As a result (see
Figure *15*) it seems that the performance of polar orbits is slightly worse (in terms of mean errors), but it stays inside the range of random variability seen for a single case in
Figure *14*. So, we can conclude that orbital inclination does not appear to significantly change the relative navigation filter.

DOI: 10.13009/EUCASS2023-677

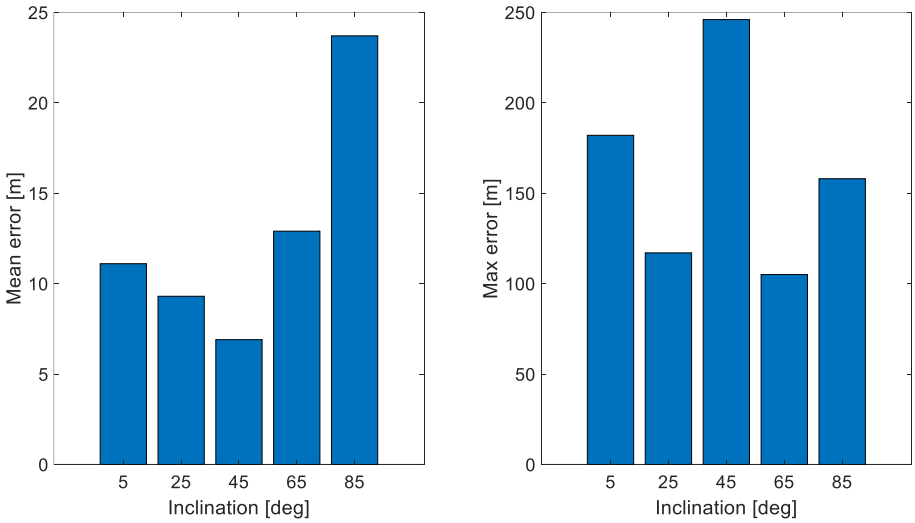

Figure 15 Effect of different inclinations of the formation orbit

Very similar results are obtained for the Scenario B, i.e., the separation of a lander from an orbiter, with increasing relative distance. The error norm of the estimate and of the input are shown in
Figure *16*. The mean value is 27m for the estimate (with respect to 32m of the input: -15%) and the maximum value is 275 m (with respect to 521 m of the input. -47%).

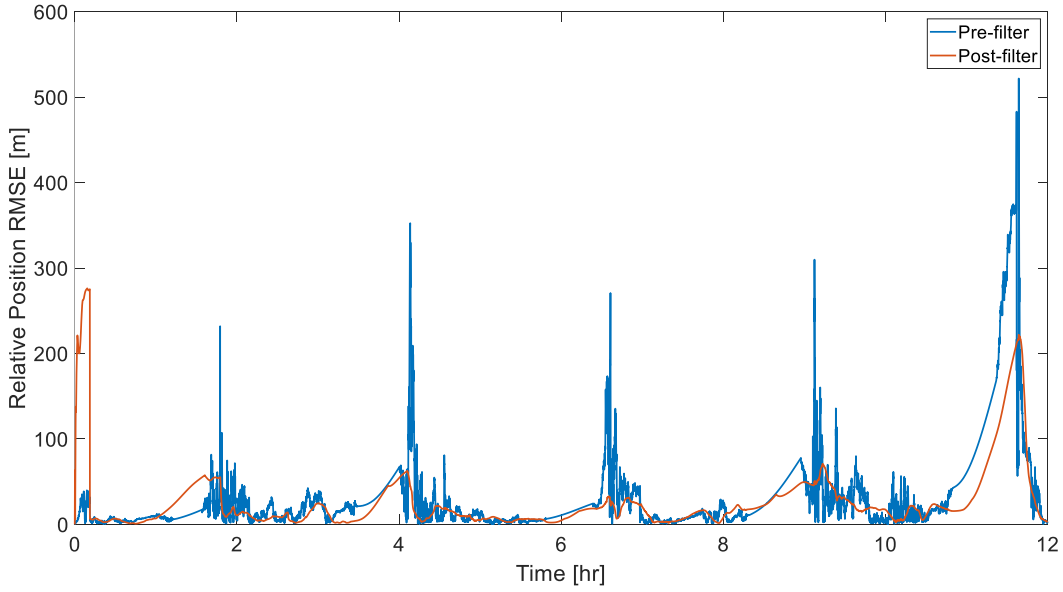

Figure 16 : Norm of the error of the input and estimated relative position: drifting formation case.

The performance in the case of Scenario C, relevant to a train formation with a large 300 km separation, is instead different and calls for some explanation. The true trajectory, the trajectory estimated after first navigation filter stage and the final relative estimate are plotted in
Figure *17*. In this case the maximum error is still improved (146m for the estimate vs 282m for the input), but the mean error of the error is worst: 41m for the estimate versus 26m for the input. This happens because for large distances between the satellites, the differential perturbations – correctly evaluated in the orbital propagation by the ”true” dynamics, are much more important, but they are neglected in the present implementation of the filter.

DOI: 10.13009/EUCASS2023-677

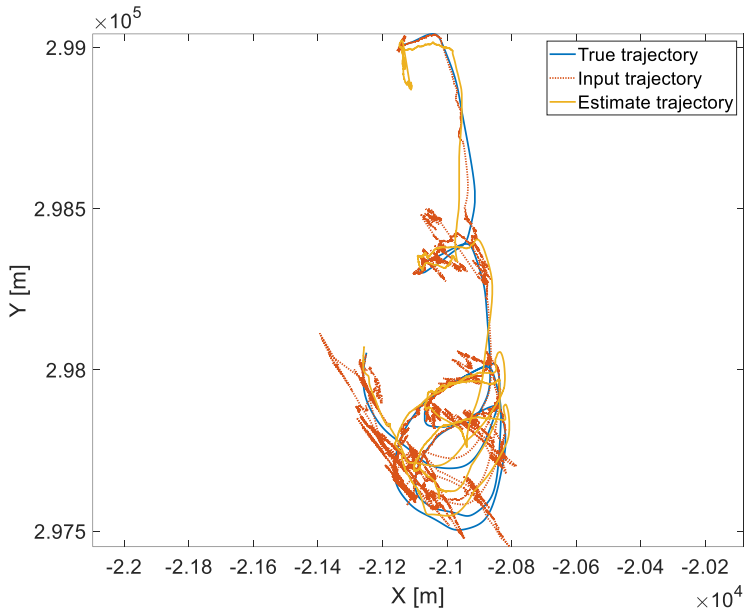

Figure 17 : True trajectory of the train formation, together with input trajectory and estimate trajectory

The simulation has been repeated for difference initial along-track distances. It is possible to see (
Figure *18*) that the maximum error of the estimate is always far smaller than the maximum error of the input. Concerning the mean error, instead, the estimates are more accurate than the input only for distances of the order of 150km or less. For larger distances, more detailed dynamic models for the prediction, including differential perturbations, should be implemented to improve the accuracy.

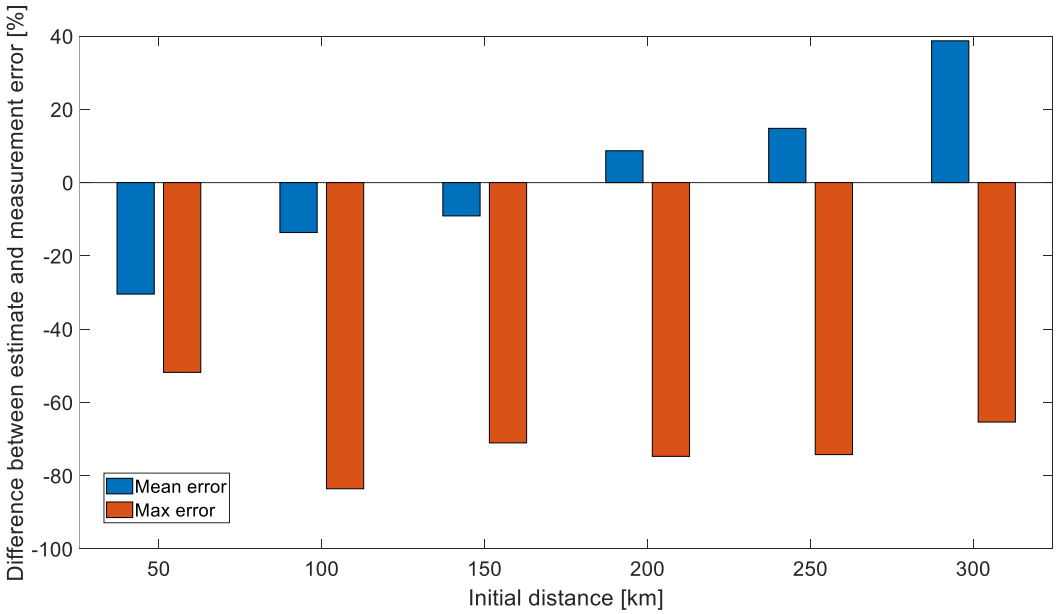

Figure 18 : Mean and maximum errors for train formations with different initial distances

6. Conclusions

A GNSS system that provides navigation services for lunar rovers and orbiters is currently being investigated by major space agencies, with particular focus on regions of greatest scientific interest, i.e., the south pole of the Moon. In this research work, the possibility of further exploiting this service as a navigation system for the formations of satellites - or for combined spacecraft operations - in the cislunar space has been analysed.

DOI: 10.13009/EUCASS2023-677

A cascade filter architecture is implemented to estimate the state of the satellite in the lunar inertial reference frame in the first step and then the relative state in an orbital frame in the second one. The main focus is on the performance in terms of relative position as a function of different orbital parameters and formation trajectories.
The results show that the dual-stage filter is able to significantly reduce, in particular, the maximum errors in relative state estimation caused by a periodical outage of navigation satellites. One factor playing a crucial role in obtaining this promising performance is the careful modelling of the error covariance matrix of the input to the second filter, which has been realized by applying an unscented transformation to the inertial positions estimates.
Integration with other navigation sensors, such as inter-satellite links and visual navigation, could further improve the presented performance, which is appealing even under the current simplified hypotheses about hardware and sensor noise, and even when taking into account the limited number of the cases studied. Indeed, more extensive investigations are needed to consolidate and extend the results to a wider variety of scenarios, including the case of rovers moving on the lunar surface.

References

[1] Smith, M. et al. 2020. The Artemis Program: An Overview of NASA's Activities to Return Humans to the Moon. In: *2020 IEEE Aerospace Conference Proceedings.*

[2] Nie, T., Gurfil, P., and Zhang, S. Lunar Satellite Formation Keeping Using Differential Solar Radiation Pressure. *J. Guid. Control Dyn.* 43 (published online).

[3] Sirbu, G., Leonardi, M., Stallo, C., and M. Carosi. 2023. Evaluation of different satellite navigation methods for the Moon in the future exploration age. *Acta Astronaut.* 208:205–218.

[4] Israel, D., Mauldin, K.D., Roberts, C.J., and J.W. Mitchell. 2020. LunaNet: a Flexible and Extensible Lunar Exploration Communications and Navigation Infrastructure. In: *IEEE Aerospace Conference Proceedings.*

[5] https://www.esa.int/Applications/Telecommunications_Integrated_Applications/Moonlight, accessed 24/05/23.

[6] Iannone, C., Carosi, M., Eleuteri, M., Stallo, C., Di Lauro, C. and D. Musacchio. 2021. Four satellites to navigate the Moon's South Pole: An Orbital Study. In: *34th International Technical Meeting of the Satellite Division of the Institute of Navigation - ION GNSS+ 2021*.

[7] Giordano, P. et al. 2021. Moonlight navigation service - how to land on peaks of eternal light. In: *Proceedings of the 72nd International Astronautical Congress – IAC*.

[8] Sirbu, G., Leonardi, M., Carosi, M., Di Lauro, C., and C. Stallo. 2022. Performance evaluation of a lunar navigation system exploiting four satellites in ELFO orbits. In: *IEEE 9th International Workshop on Metrology for AeroSpace - MetroAeroSpace*.

[9] Grenier, A. 2022. Positioning and Velocity Performance Levels for a Lunar Lander using a Dedicated Lunar Communication and Navigation System. *Navig. J. Inst. Navig.*, Vol. 69, No 2.

[10] Rodriguez, F. et al. 2023. Analysis of PNT Algorithms and Related Performance for Lunar Navigation Service Users. To appear in: *36th International Technical Meeting of the Satellite Division of the Institute of Navigation, ION GNSS+ 2023*.

[11] Zarchan, P., and H. Musoff. 2000. Fundamentals of Kalman filtering: a practical approach. *AIAA Prog. Astronaut. Aeronaut.* 190.

[12] Clohessy, W.H., and R.S. Wiltshire. 1960. Terminal guidance system for satellite rendezvous. *J. Aero. Sci.* 27: 653–678.

[13] Sabatini, M., and Palmerini, G.B. 2008. Linearized Formation-Flying Dynamics in a Perturbed Orbital Environment. In: *IEEE Aerospace Conference Proceedings*.

[14] Vallado, D.A. 1997. *Fundamental of Astrodynamics and Applications*. 4th ed., Microcosm Press.

[15] Gaias, G., Ardaens, J.S., and O. Montenbruck. 2015. Model of J2 perturbed satellite relative motion with time-varying differential drag. *Celest. Mech. Dyn. Astr.*, 123:411–433.

[16] Reali, F., and G.B. Palmerini. 2008. Estimate Problems for Satellite Clusters. In: *IEEE Aerospace Conference Proceedings*.

[17] Simon, D. 2006. *Optimal State Estimation: Kalman, H-inf and Nonlinear Approaches*. Wiley Interscience.